TECHNICAL UNIVERSITY OF CLUJ-NAPOCA

ACTA TECHNICA NAPOCENSIS

Series: Applied Mathematics, Mechanics, and Engineering
Vol. 67, Issue Special IV, August, 2024

EXPERIMENTAL DETERMINATION OF DEPENDENCES BETWEEN SELECTED IMAGE CAPTURING SETUP PARAMETERS AND THE QUALITY OF THE REGULAR RELIEFS 3D TOPOGRAPHIES

Stoyan SLAVOV, Lyubomir Si Bao VAN, Boris NIKOLOV

Abstract: *Determining the topography of the regular reliefs made using ball burnishing process is difficult using traditional approaches because most optical topography measurement systems are not designed for measurement of topography areas of such scale. The known contact methods also do not offer many advantages due to them measuring the topography profile in just one section. A hybrid optical and contact-based method which is better suited for such nontraditional topographies is studied. Some of image capturing parameters such as the topography illumination, how it filtered and levelled are not researched in deep yet. In the present work, these parameters are studied using a Taguchi experimental design and are subjected to verification by using a contact topography measurement method. Based on the obtained results from the experimental research, conclusions are made at the end of the work about the influence of the factors over the quality of regular micro reliefs images.*

Key words: *ball burnishing; regular micro-reliefs; surface topology, three-dimensional surface topography representation*

1. INTRODUCTION

There are different types of finishing machining operations and their impact on the finished parts surfaces is varied. Whilst all operations change the surface topology, most of them are concerned with achieving lower roughness parameters by cutting the surplus material. Among the existing finishing operations, however, there is a certain class of finishing processes, such as deep rolling, rolling, ball and diamond burnishing, which can be used to modify the surface layer characteristics using plastic deformation in cold state of material. This class of operations includes a variant in which the deforming element is a hard ball that follows a complex toolpath called “ball burnishing” (BB) [1, 2, 3, 4]. Using that process as finishing operation, it is possible some specific regular reliefs (RR) to be formed onto finished surface (see Fig. 1) that have distinctive topography in comparison with other traditional finishing methods as finishing turning, milling, grinding, lapping, etc. The topography height of the RRs boundaries could reach several dozen micrometers while in the lateral direction one single relief’s cell dimensions could exceeds 1500, μm. The inner surface, closed inside of the RR’s cell usually has roughness height below to 0.4 μm, according to the Ra-criterion (ISO 21920-2). The RRs obtained by ball burnishing provide a range of benefits, including improved surface finish, increased hardness, enhanced lubricant retention and wear resistance, reduced friction and dimensional stability, making it a valuable process in various industrial applications.

Using standardized methods as defined in ISO 21920 and ISO 25178-6, for surface roughness and/or waviness measurement of the RRs surface topology is challenging, as contact methods are mainly based on stylus-based devices that work in a single section. While this is appropriate for capturing stochastically distributed topography irregularities, applied to RRs this could produce substantially different profilograms depending of the specific section

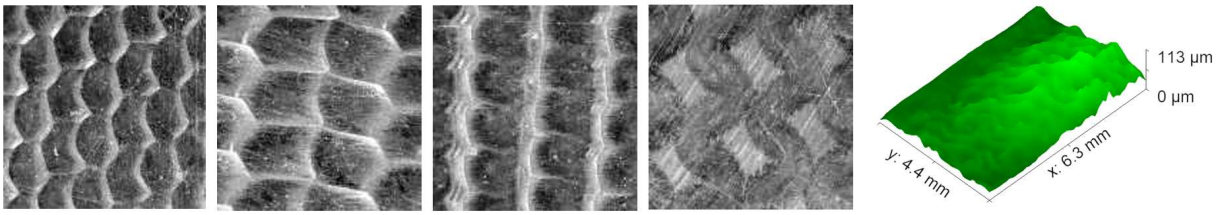

Fig. 1. 2D square (5 × 5 mm) images of RRs formed by BB operation: a) Specimen 1: complete RR with small cells; b) Specimen 2: complete RR with large cells; c) Specimen 3: partial RR without islands with former texture; d) Specimen 4: partial RR having islands with former texture; e) a 3D topography of complete RR with small cells captured by SEM.

that is measured [5]. A possible solution is tracing many parallel profilograms with a small lateral distance between them, in order the measured surface area to be covered. The productivity of such topography measurement approach however will be very low and time consuming.

There are several noncontact scanning techniques designed to improve the surface three-dimensional representation and topography characteristics measuring. The most spread in practice among them are as follow [6 – 14]:

- Optical profilometry uses light interference patterns to measure surface height variations;
- Confocal microscopy that can be light or laser based. These approaches focus a light source (or laser) on a specific plane, allowing only in-focus light to be collected;
- Atomic force microscopy (AFM) approach uses a sharp tip to scan the surface, measuring forces between the tip and the sample surface;
- White light interferometry (WLI) utilizes interference patterns generated by white light to measure surface heights. A light beam is used with very short coherence length, which is split into two additional beams. One of them is directed to the sample while the other one is directed towards a smooth reference mirror. After the light beams are reflected by the sample and by the reference mirror, they are recombined and transmitted to an array camera. In this way, a topographic image of the surface can be obtained.
- Structured light scanning (SLS). In this approach known patterns are projected onto the surface and the deformations in the patterns are measured to reconstruct the topography;
- X-ray microscopy uses X-rays to penetrate the sample and create detailed 3D images, especially when the specimens have internal features or structures;
- Scanning electron microscopes (SEM) creates topography images by using a high-energy beam of electrons directed onto a specimen's surface while scanning it in a zig-zag manner. SEMs provide high surface sensitivity with resolutions usually ranging from 1 to 10 nm.

The common advantages of the above methods for non-contact topography measurement, are the higher vertical resolution, combined with faster scanning and automatic data acquisition of measurements. Respectively, the main disadvantages are the high complexity of such equipment and therefore the high acquisition and maintenance cost for smaller laboratories or businesses. Analyzing and interpreting the measured data often is challenging and specialized software may be required for topography characterization. Optical methods also may be sensitive to changes in environmental conditions such as temperature and humidity or scanned surface condition, potentially affecting the accuracy of measurements.

For example, a topography image of a typical RR obtained by vibratory ball burnishing operation is captured by SEM device, model SU1510 (Hitachi High Technologies America, Inc.) and reconstructed to a 3D topography using Alicona software (Alicona imaging, GmbH). The SEM device is adjusted to scan the RR pattern within its maximal scanning area scope, in order to capture as many RRs cells as possible. After removing the background and smoothing by Gaussian filter, the resulted image is shown in Fig. 1, e. As can be seen the RR's topography heights are smaller and unevenly

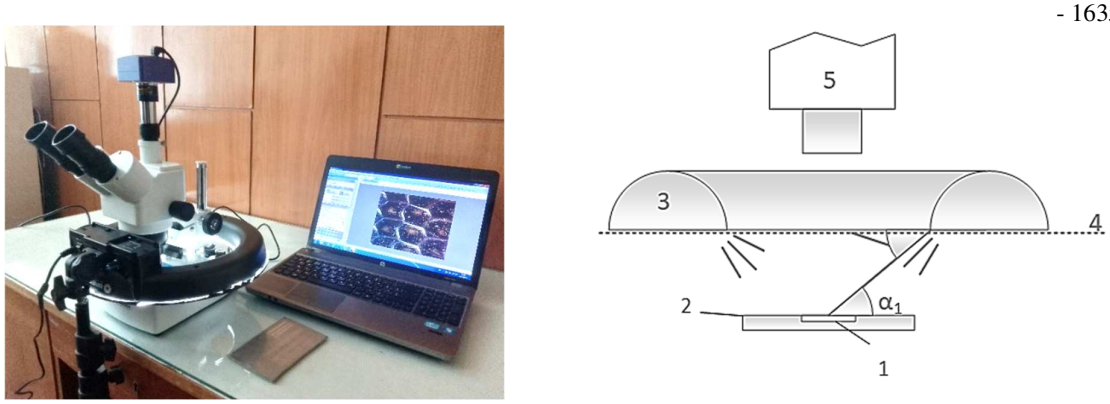

a) b)

Fig. 2. a) A setup for 2D image capturing of surfaces with RR's; b) Schematic diagram of the RR's topology imaging setup: 1- a specimen with RR; 2 – the microscope table; 3 – the halo lamp; 4 – the plane of the inner diameter of the halo lamp; 5- a CMOS high resolution digital camera.

distributed across the scanned area, which does not correspond to the actual RR topography (see Fig. 1, a). The possible reason for such results could be the fact that SEM devices are designed to capture surface textures with nano-metric heights and scan surface areas with small lateral dimensions [8, 9]. In the case of RRs, however the nano-metric precision in topography representation is not crucial, due to their large size.

Based on the above reason, a hybrid approach for 3D topology reconstruction of RRs, using 2D digital images, captured by high resolution camera and two single profilograms measured (by the contact method) in two perpendicular sections of the surface [5] is studied. The sections for profilograms measuring are selected optimally by specially developed algorithm. It iterates the rows and columns from the 2D image and compare them with profilograms measured to determine the maximal signal correlation rate. On that basis, the row and column with highest score obtained are selected as optimal match. Then the 2D image pixels grey levels are scaled with a coefficient calculated as ratio between the initial pixel grey-value and the ultimate height of the profilogram measured. Although some of the hybrid methodology parameters have been investigated, specifically the most suitable measures used in the algorithm, the questions related to the optimal conditions in which the 2D images of RRs are captured is still not researched in deep enough. Hence, the main goal of the present work is to research the factors, which affect significantly over the 2D images captured and processing conditions in order to obtain their optimal settings.

2. METHODS AND MATERIALS

2.1 2D-image capturing setup description

The RRs 2D images capturing setup is shown in Fig. 2, a, b. It consist of a trinocular head microscope with a high-resolution 14-megapixel CMOS (Levenhuk Inc.) digital camera (see pos. 1 in Fig. 2, a) attached, which is used as an image capturing device. In order to avoid unwanted reflections a diffuse light source (see pos. 3 in Fig. 2, b) based on circular video lamp (or so-called “halo-lamp“) is used. If the light source is positioned at high or low levels, it is possible to simulate the conditions of a sunrise or sunset in the mountains. Thus, the RRs topography peaks will be more brightly illuminated, and the valleys will remain dark. This approach provides greater difference in the topology illumination of the peaks and valleys of the RRs pattern, and therefore more clear distinction between them.

The RRs topographies is captured as raster 8- bit greyscale images in bitmap (BMP) format. The light incidence angle α_1 (see Fig. 2, b) is the first important parameter, which have impact over the quality of the obtained image. It can be determined by trigonometric calculation, taking into account the inner diameter of the circular lamp and the distance between the light emitting plane and the top surface of the RR specimen. In addition, the light intensity can be tuned precisely by adjusting the power supply of the lamp.

2.2 2D-image pre-processing

The raw 8-bit grey scale RRs topology image often has sharp peaks in some pixels due to reflections caused by fine surface defects, such as scratches, residual roughness from previous machining, dust, etc. They could cause errors with the heights scaling algorithm work, and therefore they should be filtered from the raw captured image. For that purpose, a Gaussian filter approach [15] is used to smooth the single peaks from the raw images. The window size of the Gaussian filter used is the second factor in the current research. To remove the impact from the ambient light sources the digitalized RR topography image could be leveled using a mean plane, obtained by Least Squares Method (LSM) fitting [16], [17], or by polynomial background subtraction. The type of levelling applied - mean plan or polynomial background subtraction is the third factor of the investigation.

2.3 Similarity degree assessment between single row /column from the RRs image and measured RRs topography profilograms

In order to scale properly the heights of the pixels from RRs image using the information from the measured single profilograms in the sections of the surface topography, the search of best-match algorithm is used [5]. To determine the best-matched pair - "measured profilogram – RRs image row (or column)" the algorithm uses a signal cross-correlation evaluation approach [18], by which a coefficient of correlation $\rho_{xy}(m)$ is defined that can be calculated with following equation:

$$\rho_{xy}(m) = \frac{\frac{1}{N}\sum_{i=1}^{N}(x_{i-m}-\bar{x})\cdot(y_i-\bar{y})}{\sqrt{\left(\frac{1}{N}\sum_{i=1}^{N}(x_i-\bar{x})^2\right)\cdot\left(\frac{1}{N}\sum_{i=1}^{N}(y_i-\bar{y})^2\right)}}, \quad (1)$$

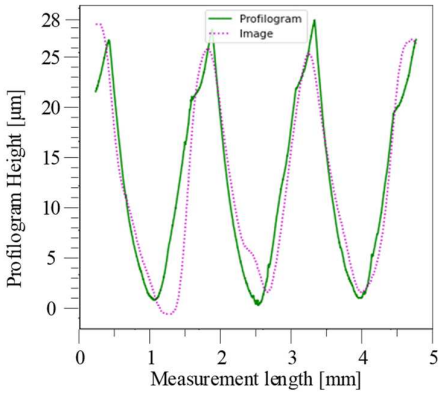

Curve Correlation coeff: 0,993968

a)

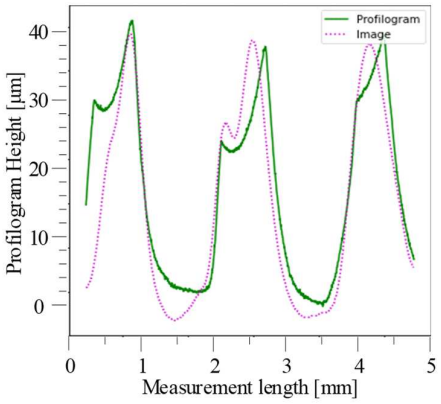

Curve Correlation coeff: 0,987795

b)

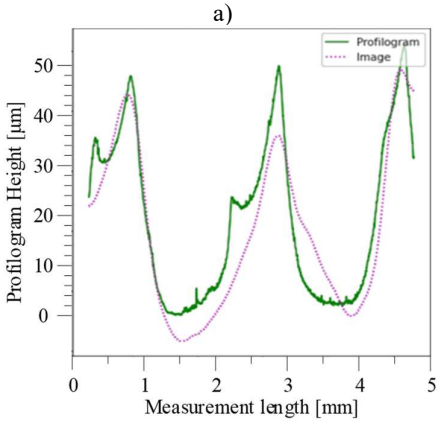

Curve Correlation coeff: 0,989539

c)

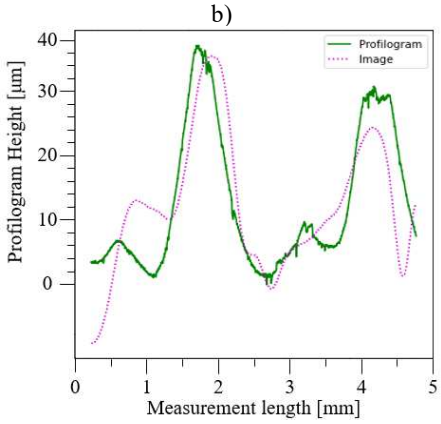

Curve Correlation coeff: 0,993005

d)

Fig. 3. Best matched measured profilogram and RRs image row/column, according to the ρ_{xy} coefficient for: a) Specimen 1; b) Specimen 2; c) Specimen 3; d) Specimen 4.

where: m— is the phase shift between x and y vectors' elements; x_i—is a vector, which contains the measured profilogram heights at position i; $\bar{x}$— is the average height of the

measured profilogram; y_i—is a vector, which contains the RRs image row (or column) heights at position i; $\bar{y}$— is the average height of the RRs image rows (or columns). N—the number of the image row vector's elements (i.e., row pixels).

An exemplar result from the algorithm of match searching can be seen in Fig. 3. It is clear that a perfect match between the profilograms measured and the RRs image rows/columns identified as "best matched" is not possible, due to stochastic factors influence (or "noise") that are depend on the image capturing condition, and the settings of the preprocessing carried out on it. Therefore, it is important to research which of these factors have significant impact and how exactly affect the degree of matching the both profiles curves, assessed by the coefficient of correlation ρ_{xy} (see Eq. 1).

3. EXPERIMENTAL RESEARCH OF THE FACTORS SIGNIFICANCE AND IMPACT

3.1 Experimental design description

An experimental design is chosen that includes the following three controlled factors: the light incidence angle α_1, the window size WS of the Gaussian filter, and type of image levelling applied: mean plan (MP) or polynomial background subtraction (PBS). The signal cross-correlation coefficient ρ_{xy} is used as response factor. In order to minimize the numbers of experiments a Taguchi L8 experimental design is used [19]. First two controllable factors have two level of variation – low and high, and the third one has two states – MP and PBS. The signal cross-correlation coefficient ρ_{xy} values are determined using equation (1) for each of the controllable factors combination. The controlled factors values and those obtained for the response parameter are shown in Table 1.

3.2 Experimental specimens description

The experimental specimens used for the present study is made of 2024-T6 aluminum alloy. They are four and have four types of RRs patterns with different size of the plastically deformed cells. The first two of them have fully regular reliefs, which means that the plastically deformed traces fully covers whole surface, and the second two have partially regular reliefs formed, i.e. there are areas with roughness obtained by the previous machining operation between the traces.

The RR patterns with dimensions of 30 × 30 mm is created using BB-operations on a CNC milling machine HAAS, TM-1, equipped with a tool for ball burnishing [20]. The deforming force applied is 700 N, the feed rate is 300 mm/min, and the spherical deforming tool has diameter of 14 mm. The toolpaths were calculated and converted into NC code using the corresponding methodology for flat surfaces [21]. The RR profilograms were measured using a Mitutoyo, America Corporation, USA, and model Surftest SJ-310 roughness tester, which has a 5 µm tip radius stylus. The Gwyddion [22] is used for preprocessing the raw RRs images (see subsection 2.2)

Table 1

Taguchi L8 experimental design and results

№	Taguchi L8 experimental design			Results obtained for the coefficient of correlation ρ_{xy}			
	Angle of incidence light, [deg.]	Gaussian filter window size, [pixel]	Type of image leveling	Specimen 1	Specimen 2	Specimen 3	Specimen 4
1	1,27	10	MP	0,989498	0,981473	0,985975	0,983020
2	1,27	10	PBS	0,988345	0,982339	0,989156	0,987099
3	6,34	25	MP	0,993125	0,987795	0,982948	0,982595
4	6,34	25	PBS	0,993968	0,985210	0,984756	0,986708
5	1,27	25	MP	0,992204	0,984752	0,985081	0,985123
6	1,27	25	PBS	0,992711	0,984280	0,989539	0,993005
7	6,34	10	MP	0,989280	0,987486	0,983716	0,981652
8	6,34	10	PBS	0,988861	0,986875	0,984243	0,982473

Table 2

ANOVA results for the regression equations (2) to (5)

Source	DF	Specimen 1			Specimen 2			Specimen 3			Specimen 4		
		Contrib.	F-Value	P-Value	Contrib.	F-Value	P-Value	Contrib.	F-Value	P-Value	Contrib.	F-Value	P-Value
Regression	3	99,18%	161,11	0,0005	86,13%	14,25	0,048	89,58%	11,46	0,020	86,28%	8,38	0,034
Angle	1	0,09%	0,42	0,553	70,02%	11,73	0,027	59,55%	22,85	0,009	27,91%	8,13	0,046
Gauss	1	97,22%	473,79	0,001	3,50%	0,59	0,487	0,18%	0,07	0,808	22,10%	6,44	0,064
Levelling	1	1,87%	9,11	0,039	12,61%	13,44	0,045	29,85%	11,45	0,028	36,27%	10,57	0,031
Error	4	0,82%	-	-	13,87%	-	-	10,42%	-	-	13,72%	-	-
Total	7	100,00%	-	-	100,00%	-	-	100,00%	-	-	100,00%	-	-

3.3 Results from the experimental research conducted

The results obtained for the coefficient of correlation ρ_{xy} for all experimental design plan combinations, and for all four specimens with RRs are shown in Table 1. In order to analyze the obtained results, regression analyses and analyze of variance (ANOVA) techniques are used.

4. ANALYSES AND DISCUSSION OF THE EXPERIMENTAL RESULTS OBTAINED

4.1 Regression analyses

Four regression equations are derived, based on the results for the coefficient of correlation ρ_{xy} shown in Table 1. They are as follow:

- For the specimen 1:

$$\rho_{xy}(Angle, Gauss, MP) = 0{,}985958 + 0{,}000023 \cdot Angle + 0{,}000267 \cdot Gauss + 0{,}000556 \cdot MP \quad (2)$$

- For the specimen 2:

$$\rho_{xy}(Angle, Gauss, MP) = 0{,}981 + 0{,}000716 \cdot Angle + 0{,}000054 \cdot Gauss + 0{,}0007 \cdot MP \quad (3)$$

- For the specimen 3:

$$\rho_{xy}(Angle, Gauss, MP) = 0{,}98979 - 0{,}000695 \cdot Angle - 0{,}000013 \cdot Gauss - 0{,}002493 \cdot MP \quad (4)$$

- For the specimen 4:

$$\rho_{xy}(Angle, Gauss, MP) = 0{,}98626 - 0{,}000731 \cdot Angle + 0{,}000220 \cdot Gauss - 0{,}00422 \cdot MP \quad (5)$$

In Table 2 the ANOVA assessment of the statistical significance (at confidence level of 5%) of the coefficients before the three controllable factors for the four specimen tested are given, along with their F- values and P-values calculated. As can be seen from them, the regression error (0.82%) is smallest for the specimen 1, and have highest level (13.87%) for the specimen 2 (see Fig. 4). For the first specimen the coefficients before Gauss filter window size and the method of levelling have statistical significance, while those before the angle of light incidence is statistically insignificant. For the second specimen a statistical significance have coefficients before angle of light incidence and the method of levelling. The third and fourth specimens again have statistically significance of the coefficients before angle of light incidence and the method of levelling, while the Gauss window size factor is statistically insignificant. Therefore, the statistically insignificant coefficients in (2) to (5) can be equaled to zero, and the regression equations can be simplified to those that are statistically significant.

4.2 Response table of means and main effects plots

Using the derived regression equations (without zeroing the statistically insignificant coefficients) for the four specimens with RRs, a response table of means can be calculated that shows how strong the effect of the factors is over the cross-correlation coefficient. Calculated values, using Minitab software are given in Table 3.

As can be seen from Table 3, calculated effects of the three researched factors shows that for the three of the specimens with RR (1, 2 and 3) the Angle of incidence light factor has the first rank of significance because sum of ranks for the four specimens is 5. This means that the Angle of incidence light factor affects most significantly to the coefficient of correlation ρ_{xy}. Type of image leveling holds the second rank of significance over the coefficient of correlation ρ_{xy}, because it has a score 8 for sum of ranks. The

smallest effect has the Gaussian filter window size factor with score 11.

From the main effects plots, shown in Fig. 4, a – d, the influence direction from low to high values of the three factors for the different specimens with RR can be seen. When the specimens have fully regular reliefs, the angle of incidence light should be kept on his higher level (i. e. 6.34 degree), and opposite if the RRs is partial, it must be set on its lower level (i. e. 1.27 degree).

The effects graphs shows that the levelling of the image using mean plan method has better effect on the coefficient of correlation ρ_{xy} than the polynomial background subtraction in case of fully RR, but when there are partially RR captured the alternative approach is more suitable. The higher values of the Gaussian filter window size lead to slight increase of the coefficient of correlation ρ_{xy} in case of fully regular reliefs, but that tendency is controversial when partially regular reliefs are photographed.

4.3. Verification of the researched approach

The corresponding three-dimensional topographies of the four types of RRs derived by the described in subsection 2 approach are shown in Fig. 5, a - d. They were processed under the parameters values, which lead to the maximal coefficient of correlation ρ_{xy}, according to the effects graphs shown in Fig 4. The values of standardized criteria Sz and Sa (according to ISO 25178) which characterize the topography heights were determined using the Gwyddion software and also are shown in Fig. 5, a - d.

The same four specimens with four different types of RRs were subjected additionally to surface measuring using a CNC roughness measuring system Mitutoyo Surftest Extreme SV-3000CNC equipped with additional Y-axis that allows 3D scanning the surface topography by contact method. The measured area has the same dimensions 5 × 5 mm. The resulted 3D topographies are shown in Fig. 6, a – d, along

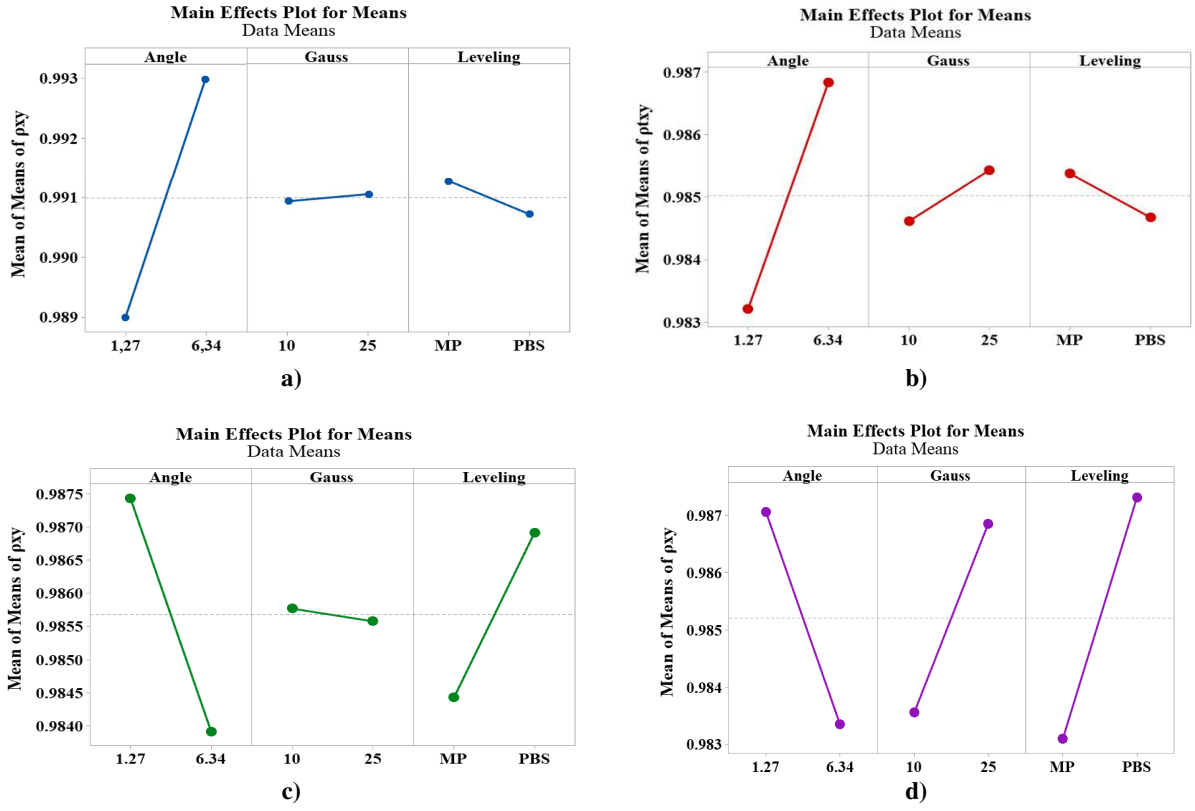

Fig. 4. Main effects plots for means for: a) Specimen 1; b) Specimen 2; c) Specimen 3; d) Specimen 4.

Table 3

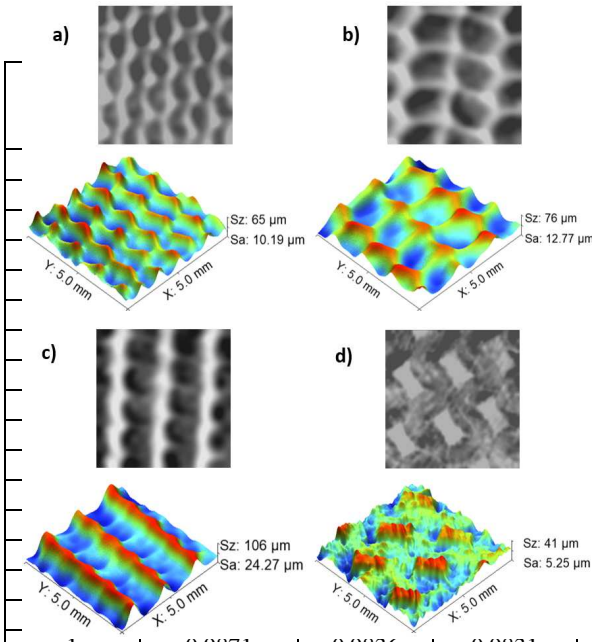

1	0,9871	0,9836	0,9831
2	0,9834	0,9869	0,9873
Delta	0,0037	0,0033	0,0042
Rank	2	3	1
Sum of ranks	**5**	**11**	**8**

Fig. 5. Three-dimensional topographies of RRs obtained by the researched approach: a) complete RR with small cells; b) complete RR with large cells; c) partial RR without islands having former texture; d) partial RR having islands with former texture.

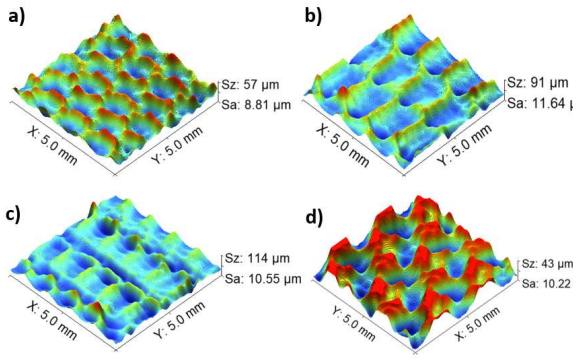

Fig. 6. Three-dimensional topographies of RRs obtained by 3D surface measuring. They are corresponds to these, shown in Fig. 5 a-d.

with obtained values for Sz and Sa criteria by Formtracepak software (Mitutoyo).

Comparing the resulting 3D topographies shown in Fig. 5 and 6, it is seen that for the first two RRs, which are complete regular, there is a higher degree of similarity, while for the third and fourth specimens, which have partial type of RRs the similarity is comparatively smaller. The obtained topography maximum heights Sz have relatively close values: the difference between two methods used varies between 2% (see Fig. 5 and 6, d) and 16% (see Fig. 5 and 6, b), depend on the type of RRs. If the topography heights are compared using Sa-criterion, it is seen that the arithmetic mean heights have comparatively close values for the complete RRs (see Fig. 5 and 6, a, b), while for the partial RRs (see Fig. 5 and 6, c, d) the difference could reach about 50%. This can be explained with the fact that complete regular reliefs have more homogeneous texture that are made of cells having more even scatter ability. The partial RRs have wider cells boundaries, which reflect the incident light more strongly and therefore they protrude more in height than in reality (see Fig. 5, c and 6, c). The presence of islands of previous topography formed by cutting operation also affects the scattering ability of partial RRs turning them into plateaus that are more elevated (see Fig. 5, d and 6, d).

5. CONCLUSION

Based on research conducted, the following conclusions can be made:

- The influence of setup parameters for two-dimensional imaging of RRs topographies, using an optical microscope to increase the cross-correlation coefficient between contact measured and image-derived profilograms is identified;
- It was found that the angle of incidence light and type of levelling have the strongest influence on the correlation coefficient, while the Gaussian filter window size has the least influence.
- The manner of influence of the researched factors is not strong affected by the type of the regular relief captured, fully or partially regular. As can be seen from Table 2, the factors: angle incidence light α and type of levelling have significant effect over RRs images for specimens 2, 3 and 4. Therefore in future research the values of the Gaussian filter window should be fixed on the high level (see Fig. 5), while the other two factors will be varied to obtain optimal topography image of RR.

• Comparative verification of the researched approach shows that it gives better results for topography heights when complete RRs are subjected to reconstruction. The measured topography heights, according to Sa criterion for partially RRs could differ significantly from the heights obtained by the researched methodology.

In conclusion, the presented methodology for 3D reconstruction of RRs topography in the current work could not be considered as an alternative to the existing methods for 3D measuring topography. At the same time, it is distinguished by its simplicity and accessibility of the used technical equipment and software for its implementation. Its application can be relevant when RRs topography should be presented as a three-dimensional representation in case of artificial neural network (ANN) training, which can be used for automatic recognition of complete RRs patterns, processed by BBs operation, which will be future work for our team.

6. ACKNOWLEDGEMENTS

The present work is funded by Bulgarian National Science Fund (BNSF), under grant contract № KP-06-N57/6, entitled "Theoretical and experimental research of models and algorithms for formation and control of specific relief textures on different types of functional surfaces", for which the authors are deeply grateful.

The authors also would like to thank to Prof. João C. C. Abrantes and Prof. Adélio Manuel Sousa Cavadas from UIDM of the Polytechnic Institute of Viana do Castelo, Portugal for their support and patience to have access to the SEM at the UIDM material science laboratory for the current research.

7. REFERENCES

[1] Ю. Шнейдер, "Эксплуатационные свойства деталей с регулярным микрорельефом," Л. Машиностроение, vol. 248, p. 3, 1982.

[2] S. D. Slavov, D. M. Dimitrov, and M. I. Konsulova-Bakalova, "Advances in burnishing technology," in Advanced Machining and Finishing, Elsevier, 2021, pp. 481–525. doi: 10.1016/B978-0-12-817452-4.00002-6.

[3] V. Dzyura, P. Maruschak, and O. Prentkovskis, "Determining Optimal Parameters of Regular Microrelief Formed on the End Surfaces of Rotary Bodies," Algorithms, vol. 14, no. 2, p. 46, Jan. 2021, doi: 10.3390/a14020046.

[4] G. Dessein, G. Dessein, and J. A. Travieso-Rodriguez, "Finishing Operations to Enhance Surface Integrity of Parts," Finish. Oper. to Enhanc. Surf. Integr. Parts, p. 182, Nov. 2023, doi: 10.3390/BOOKS978-3-0365-9285-5.

[5] S. Slavov, L. S. B. Van, D. Dimitrov, and B. Nikolov, "An Approach for 3D Modeling of the Regular Relief Surface Topography Formed by a Ball Burnishing Process Using 2D Images and Measured Profilograms," Sensors 2023, Vol. 23, Page 5801, vol. 23, no. 13, p. 5801, Jun. 2023, doi: 10.3390/S23135801.

[6] S. Van Der Jeught and J. J. J. Dirckx, "Real-time structured light profilometry: a review," 2016, doi: 10.1016/j.optlaseng.2016.01.011.

[7] Y. Hu, Q. Chen, S. Feng, and C. Zuo, "Microscopic fringe projection profilometry: A review," Opt. Lasers Eng., vol. 135, p. 106192, 2020, doi: 10.1016/j.optlaseng.2020.106192.

[8] Y. Wang, S. Ma, and L. Dong, "Review of surface profile measurement techniques based on optical interferometry," 2017, doi: 10.1016/j.optlaseng.2017.02.004.

[9] A. D. Elliott, "Confocal Microscopy: Principles and Modern Practices," Curr. Protoc. Cytom., vol. 92, no. 1, p. e68, Mar. 2020, doi: 10.1002/CPCY.68.

[10] R. Kubota, W. Tanaka, and I. Hamachi, "Microscopic Imaging Techniques for Molecular Assemblies: Electron, Atomic Force, and Confocal Microscopies," Chem. Rev., vol. 121, no. 22, pp. 14281–14347, Nov. 2021, doi: 10.1021/ACS.CHEMREV.0C01334/ASSET/IMAGES/MEDIUM/CR0C01334_0055.GIF.

[11] X. Teng, F. Li, and C. Lu, "Visualization of materials using the confocal laser scanning microscopy technique," Chem. Soc. Rev., vol. 49, no. 8, pp. 2408–2425, Apr. 2020, doi: 10.1039/C8CS00061A.

[12] F. Hidayanti and A. A. Harnovan, "International Journal of Applied Science and Engineering Review APPLICATION OF SCANNING ELECTRON MICROSCOPY: A REVIEW," 2020, Accessed: Mar. 04, 2024. [Online]. Available: http://ijaser.org

[13] W. Li, Y. Yuan, J. Yang, and L. Yuan, "Review of Optical Fiber Sensor Network Technology Based on White Light Interferometry,"

Photonic Sensors, vol. 11, no. 1, pp. 31–44, Mar. 2021, doi: 10.1007/S13320-021-0613-X/METRICS.

[14] Z. Ren, F. Fang, N. Yan, and Y. Wu, "State of the Art in Defect Detection Based on Machine Vision," Int. J. Precis. Eng. Manuf. Technol. 2021 92, vol. 9, no. 2, pp. 661–691, May 2021, doi: 10.1007/S40684-021-00343-6.

[15] A. Jain and R. Gupta, "Gaussian filter threshold modulation for filtering flat and texture area of an image," Conf. Proceeding - 2015 Int. Conf. Adv. Comput. Eng. Appl. ICACEA 2015, pp. 760–763, Jul. 2015, doi: 10.1109/ICACEA.2015.7164804.

[16] T. Chai and R. R. Draxler, "Root mean square error (RMSE) or mean absolute error (MAE)? - Arguments against avoiding RMSE in the literature," Geosci. Model Dev., vol. 7, no. 3, pp. 1247–1250, Jun. 2014, doi: 10.5194/GMD-7-1247-2014.

[17] D. Eberly, "Least Squares Fitting of Data by Linear or Quadratic Structures," Sep. 07, 2021. Available on: https://www.geometrictools.com/Documentation/LeastSquaresFitting.pdf (accessed Mar. 22, 2024).

[18] J. Benesty, J. Chen, Y. Huang, and I. Cohen, "Pearson correlation coefficient," Springer Top. Signal Process., vol. 2, pp. 1–4, 2009, doi: 10.1007/978-3-642-00296-0_5/COVER.

[19] N. C. Fei, N. M. Mehat, and S. Kamaruddin, "Practical Applications of Taguchi Method for Optimization of Processing Parameters for Plastic Injection Moulding: A Retrospective Review," ISRN Ind. Eng., vol. 2013, pp. 1–11, Jun. 2013, doi: 10.1155/2013/462174.

[20] S.D. Slavov and I.V. Iliev, "Design and FEM static analysis of an instrument for surface plastic deformation of non-planar functional surfaces of machine parts," Fiability Durab., vol. 1, no. 2, pp. 3–9, [Online]. Available: https://doaj.org/article/5d09023126684e709cca46eb394d5573

[21] S. Slavov, "An Algorithm for Generating Optimal Toolpaths for CNC Based Ball-Burnishing Process of Planar Surfaces," in Advances in Intelligent Systems and Computing, vol. 680, 2018, pp. 365–375. doi: 10.1007/978-3-319-68324-9_40.

[22] D. Nečas and P. Klapetek, "Gwyddion: An open-source software for SPM data analysis," Cent. Eur. J. Phys., vol. 10, no. 1, pp. 181–188, Feb. 2012, doi: 10.2478/S11534-011-0096-2/MACHINEREADABLECITATION/RIS.

O DETERMINARE EXPERIMENTALĂ A DEPENDENȚELOR ÎNTRE PARAMETRII DE CONFIGURARE A CAPTURĂRII IMAGINILOR SELECTAȚI ȘI CALITATEA TOPOGRAFIILOR 3D A RELIEFURI REGULARE

Rezumat: Determinarea topografiei reliefurilor obișnuite realizate folosind procesul de lustruire cu bile este dificilă folosind abordările tradiționale, deoarece majoritatea sistemelor de măsurare a topografiei optice nu sunt proiectate pentru măsurarea zonelor topografice de o asemenea scară. De asemenea, metodele de contact cunoscute nu oferă multe avantaje datorită măsurării profilului topografiei într-o singură secțiune. Este studiată o metodă hibridă optică și bazată pe contact, care este mai potrivită pentru astfel de topografii netradiționale. Unii dintre parametrii de captare a imaginii, cum ar fi iluminarea topografiei, modul în care este filtrată și nivelată, nu sunt încă cercetați în profunzime. În lucrarea de față, acești parametri sunt studiați folosind un design experimental Taguchi și sunt supuși verificării prin utilizarea unei metode de măsurare a topografiei de contact. Pe baza rezultatelor obținute în urma cercetării experimentale, la finalul lucrării se fac concluzii despre influența factorilor asupra calității imaginilor obișnuite în microreliefuri.

Stoyan SLAVOV, Department of Mechanical Engineering and Machine Tools, Technical University of Varna, sdslavov@tu-varna.bg

Lyubomir SI BAO VAN, Department of Mechanical Engineering and Machine Tools, Technical University of Varna, lubomir.van@tu-varna.bg

Boris NIKOLOV, Department of Communication Engineering and Technologies, Technical University of Varna, boris.nikolov@tu-varna.bg